

Results of the attitude reconstruction for the UniSat-6 microsatellite using in-orbit data

BATTISTINI, S <<http://orcid.org/0000-0002-0491-0226>>, CAPPELLETTI, C
and GRAZIANI, F

Available from Sheffield Hallam University Research Archive (SHURA) at:

<https://shura.shu.ac.uk/24857/>

This document is the Accepted Version [AM]

Citation:

BATTISTINI, S, CAPPELLETTI, C and GRAZIANI, F (2016). Results of the attitude reconstruction for the UniSat-6 microsatellite using in-orbit data. *Acta Astronautica*, 127, 87-94. [Article]

Copyright and re-use policy

See <http://shura.shu.ac.uk/information.html>

Results of the attitude reconstruction for the UniSat-6 microsatellite using in-orbit data

Simone Battistini^{a,*}, Chantal Cappelletti^a, Filippo Graziani^b

^a*Faculdade Gama, Universidade de Brasília, Gama, DF, Brazil*

^b*GAUSS srl, Roma, Italy*

Abstract

UniSat-6 is a civilian microsatellite that was launched in orbit on the 19th of June, 2014. Its main mission consisted in the in-orbit release of a number of on-board carried Cubesats and in the transmission to the UniSat-6 ground station of telemetry data and images from an on-board mounted camera. The spacecraft is equipped with a passive magnetic attitude control system. Gyros and magnetometers provide the information about the attitude of the spacecraft.

The importance of reconstructing the attitude motion of UniSat-6 lies in the dual possibility, for future missions, of:

- controlling the direction of ejection of the on-board carried satellites
- having an accurate pointing for remote sensing operation

The reconstruction of the attitude motion of UniSat-6 is based on the data of the on-board Commercial Off The Shelf (COTS) gyros and magnetome-

*Corresponding author

Email addresses: `simone.battistini@aerospace.unb.br` (Simone Battistini), `chantal@aerospace.unb.br` (Chantal Cappelletti), `filippo.graziani@gaussteam.com` (Filippo Graziani)

ters, downloaded at the passages over the ground station in Roma, Italy. At ground, these data have been processed with the UnScented QUaternion Estimator (USQUE) algorithm. This estimator is an adaptation of the Unscented Filter to the problem of spacecraft attitude estimation. The USQUE is based on a dual attitude representation, which involves both quaternions and Generalized Rodrigues Parameters. In this work, the propagation phase of the algorithm contains only a kinematic model of the motion of the spacecraft.

This paper presents the results of the reconstruction of the UniSat-6 attitude using on-board measurements. The results show that the spacecraft effectively stabilized its attitude motion thanks to the on-board magnetic devices.

Keywords: Attitude estimation, Unscented Quaternion Estimator

1. Introduction

UniSat-6 is the sixth civilian micro-satellite of the UniSat series. While the first four satellites of the UniSat series were established as part of the research activities at the Scuola di Ingegneria Aerospaziale of Sapienza Università di Roma since the late 1990s, the last two have been designed, built and launched by the Italian company GAUSS srl, which stemmed from the experience of the previous university years.

The UniSat platform is intended as a provider of satellite services, such as the in-orbit release of smaller satellites (e.g. CubeSats and PocketQubs) or the in-orbit test of technologies and devices [1], [2], [3]. The advantage of the solutions offered by GAUSS are the flexibility and the low cost of launches.

The UniSat platforms, in fact, are able to carry on several nano and picosatellites as a mothership, and to release them in orbit spacing them with a fixed interval in order to reduce collision risks [4]. Launch costs are kept low because the spacecrafts boarded in the UniSat share launch and administration expenses. In two missions realized in 2013 and 2014, more than 10 satellites were successfully deployed in orbit by GAUSS platforms [5], [6], [7]. One of the next objectives for GAUSS is to increase its platform capabilities in order to be able in the future to determine and control the exact release position of each daughter satellites. In order to achieve this result keeping down the costs and maintaining the simplicity of the design of the spacecraft, it is crucial to be able to determine the attitude of the spacecraft on-board the satellite with a reduced number of sensors. This paper will demonstrate how this can be accomplished with a minimum set of magnetometers and rate-gyros. Flight results from the UniSat-6 mission will be presented as well.

Rate-gyros and magnetometers measurements cannot be directly employed to reconstruct the attitude because of the noise and drift of the sensors. The attitude reconstruction, therefore, has to be based on non-linear estimation techniques. Attitude determination restrictions and requirements of UniSat-6 are typical of most general spacecraft attitude determination problems. Several solutions for this problem can be found in literature [8]. Nonlinear Filters such as the Extended Kalman Filter (EKF) have been used for decades [9]. Several representations of spacecraft attitude can be used, such as Euler angles, quaternions, modified Rodrigues parameters and others. Given the absence of singularities, quaternions are commonly employed. To avoid vio-

lations of the quaternion normalization constraint with the EKF algorithm, the so-called multiplicative quaternion approach is adopted [10].

The nonlinear filter employed in this work is the Unscented QUaternion Estimator (USQUE), proposed in [11]. This is an adaptation of the Unscented Filter (UF) [12] to the spacecraft attitude determination problem. The USQUE has already been employed in several satellite applications [13], [14], [15]. The UF is known for having several advantages over the EKF, such as smaller error in the estimation and the absence of Jacobian computations in the algorithm. The present filter uses a dual parameterization of attitude, by employing both quaternions and modified Rodrigues parameters in the algorithm.

This paper is organized as follows. Section II describes UniSat-6 mission, platform and attitude hardware. Section III introduces the attitude determination problem, describing the employed reference frames, attitude parameterization, measurements modelling and the nonlinear filter. Section IV shows the results of the attitude reconstruction from UniSat-6 real mission data. Conclusions and final comments are given in Section V.

2. UniSat-6 mission and platform

2.1. Platform

UniSat-6 is designed to match the characteristics of a low cost and reliable satellite optimized for piggy-back launches. The spacecraft is an updated version of the UniSat-5 satellite platform and it is built in reinforced aluminium and carbon fiber honeycomb panels. It is a 40 *cm* cube with a weight of 26 *kg*. After the release of the CubeSats, the weight drops to 16 *kg*. The

satellite has been designed to maintain an internal thermal range between $-10\text{ }^{\circ}\text{C}$ and $10\text{ }^{\circ}\text{C}$. Power is provided by body-mounted solar panels, which provide from 5 W (bottom panel) to 11 W (4 side panels) of electrical power. Command uplink and data downlink is provided by a communication system consisting in a UHF radio and 4 antennas. Radio-amateur frequencies are used in accordance with IARU regulations. The On-Board-Data-Handling (OBDH) is based on the ABACUS computer. ABACUS is a very low power consumption system that uses a CubeSat form factor (PC104) and that has been developed at the Scuola di Ingegneria Aerospaziale of Sapienza Università di Roma in collaboration with GAUSS [16].

A 3 Mpx camera is boarded to take pictures of the Cubesats at the ejection from the mothership and for low-resolution Earth observation images. The camera is placed on the top panel of the spacecraft. The pictures from the camera will be used throughout the paper to validate the results of the attitude reconstruction.

For the UniSat-6 mission, a passive attitude control system using permanent magnets and hysteresis rods was chosen. The ADCS systems will be described in details in Section 2.3.

2.2. Mission and operations

UniSat-6 was launched on June 19th, 2014 at 21:11:11 CET from the Dombarovsky Cosmodrome in Yasny, Russia, on board a DNEPR-1 rocket from the Russian company Kosmotras. Communications with ground were acquired 90 minutes after the launch, when passing over Italy. Table 1 shows UniSat-6 orbital parameters at the injection. The orbit is almost Sun Synchronous and it was reached 15 minutes after the launch [17].

Table 1: **UniSat-6 orbital parameters at the injection**

Altitude	620 <i>km</i>
Eccentricity	$\simeq 0^\circ$
Inclination	97.9°
Separation Angular Velocity	$< 18 \text{ }^\circ/s$

UniSat-6 main task was the in orbit release of the boarded CubeSats. The released spacecrafts were Tigrisat (3U), Lemur-1 (3U), AntelSat (2U) and Aerocube 6 (1U) for a total deployment volume capability of 9U. The deployment of the satellites took place 25 hours and 38 minutes after the launch and it was initiated by an autonomous system with a dedicated battery. Confirmation of the deployment was given 15 minutes after release when the spacecraft passed the over ground station in Italy. All the deployed CubeSats communicated with ground, confirming the good health of all the satellites and the full accomplishment of the deployment operations [18].

Other mission objectives were the test of the on-board payloads and sub-systems, such as the new telecommunication system, the solar panels, the new electronic bus and the on-board camera. All the collected data from the sensors and the telemetry are stored and sent to ground on a daily basis. Some of the recorded anomalies in the data were correlated to the inherent effects of the space environment, such as Single Event Upsets (SEU), that have been observed acting on the flash memory or some sensors. SEU effects on attitude measurements and reconstruction will be described in Section 4. UniSat-6 has been regularly operated since its in-orbit release in June 2014.

The ground station in Roma managed to establish a two ways effective communication with it few minutes after launch. [19].

2.3. ADCS hardware

UniSat-6 is equipped with various devices for attitude determination and control. Attitude related measurements are given by two sensors, a rate gyro (L3GD20) and a magnetometer (HMC5883L). The L3GD20 is a low-power MEMS three-axis angular rate sensor, used in terrestrial applications such as video-games, GPS navigation and robotics. The HMC5883L is a three-axis compass that enables 1° to 2° compass heading accuracy.

UniSat-6 does not have an active attitude control, but relies on a passive magnetic control to stabilize the spacecraft. Since UniSat-6 does not have strict requirements on pointing, the choice of passive magnetic control is a good compromise between simplicity, cost and performances. The magnetic torque is generated by 4 permanent magnets and 17 hysteresis rods. The magnets are made of Alnico-5 and give a total magnetic dipole of 5 Am^2 . They are placed along the \hat{y}_b axis of the satellite. The 17 hysteresis rods are spread on the 3 axes: 8 along the \hat{x}_b axis, 1 along the \hat{y}_b axis and other 8 along the \hat{z}_b axis. Fig. 1 shows the position of these devices on board of UniSat-6 in accordance with the axes defined by the on-board magnetometer for expressing its measurements. Nevertheless, these axes do not coincide with the reference frame that will be used to define the results of this paper, which will be described in Section 3.1.

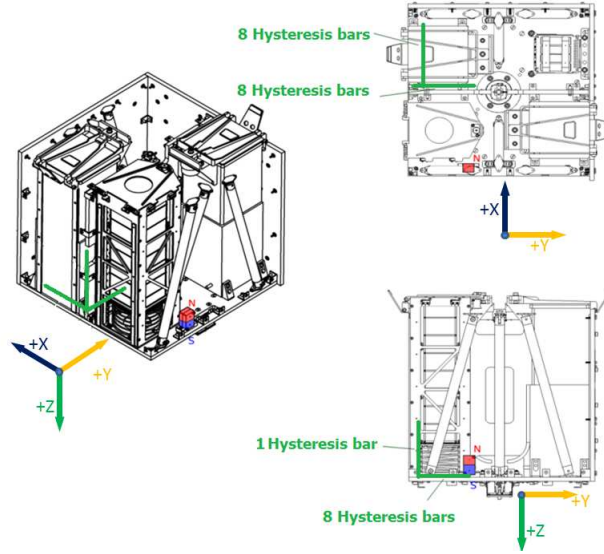


Figure 1: **Position of magnets and hysteresis rods (magnetometers defined axes)**

3. Attitude determination

3.1. Reference frames

In order to represent the orientation of the spacecraft, three reference frames are introduced. The first reference frame $\left(\hat{C}_1 \ \hat{C}_2 \ \hat{C}_3 \right)$ is an Earth Centred Earth Fixed (ECEF) frame. The first two axes are contained in the equatorial plane of the Earth, with the first directed from the centre of the Earth to the Greenwich meridian. The third axis is directed from the centre of the Earth to the North Pole. The second axis completes the orthogonal reference frame.

The second reference frame $\left(\hat{r} \ \hat{\theta} \ \hat{h} \right)$ is the orbital frame, shown in Fig. 2, with origin in the centre of mass of the spacecraft. The first axis is directed along the radial of the orbit. The second axis is directed as the tangential

velocity of the orbit. The third axis is directed along the perpendicular to the orbital plane.

The third reference frame $\left(\hat{x}_b \ \hat{y}_b \ \hat{z}_b \right)$ is the body-axes reference frame, represented in Fig. 3. The reference frame has its origin in the centre of mass of the spacecraft. The \hat{x}_b and \hat{z}_b axes exit from the side panels of the spacecraft. The \hat{y}_b is pointing towards the direction of the release of the CubeSats (i.e. parallel to the deployers). This reference frame is different from the one shown in Fig. 1, which is related to the inner axes of the magnetometer.

The aim of this paper is to analyze the orientation of the body frame with respect to the orbital frame because the latter constitutes the main reference frame for the analysis of spacecraft attitude control algorithms. This orientation is easily expressed by means of the Euler angles ϕ , θ , ψ in the sequence 3-2-1, defined as in Fig. 2. In order to obtain the Euler angles, the orientation of the ECEF frame with respect to the orbital frame and the orientation of the body frame with respect to the ECEF frame need to be calculated. The orientation of the ECEF frame with respect to the orbital frame is given by three successive rotations as follows:

1. a rotation about the \hat{C}_3 axis of the ECEF frame by the Right Ascension of the Ascending Node (RAAN) Ω
2. a rotation about the new \hat{C}_1' axis by the argument of latitude u
3. a rotation about the new \hat{C}_3'' axis by the inclination i

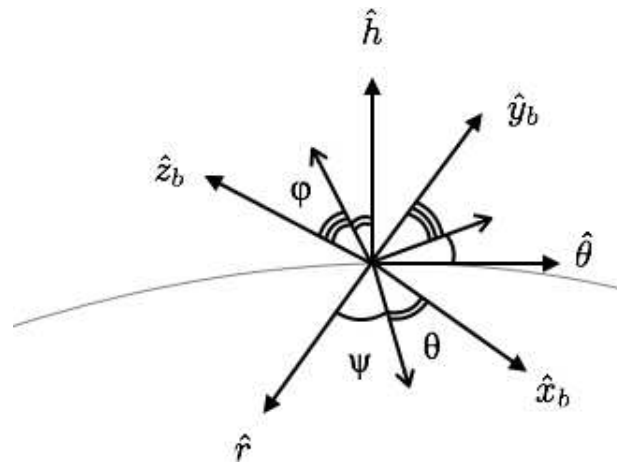


Figure 2: Euler angles and orbital frame

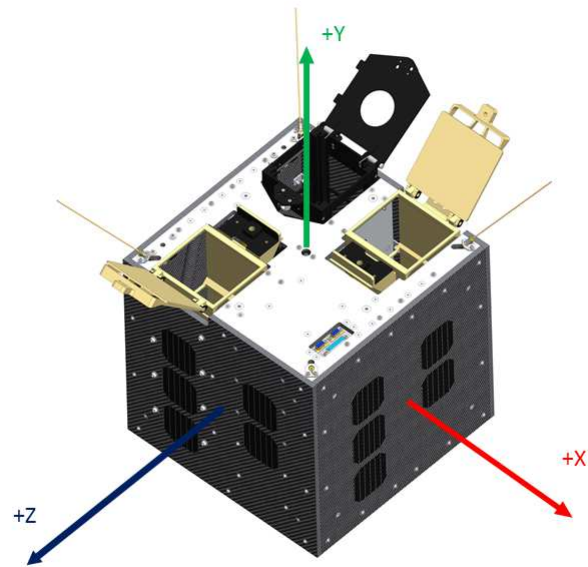


Figure 3: Body-axes reference frame

The rotation matrix that represents the orientation is given by the multiplication of the three rotation matrices T_1 , T_2 , T_3 .

$$\begin{pmatrix} \hat{C}_1 \\ \hat{C}_2 \\ \hat{C}_3 \end{pmatrix} = T \begin{pmatrix} \hat{r} \\ \hat{\theta} \\ \hat{h} \end{pmatrix} = T_1 T_2 T_3 \begin{pmatrix} \hat{r} \\ \hat{\theta} \\ \hat{h} \end{pmatrix} \quad (1)$$

$$T_1 = \begin{pmatrix} \cos \Omega & -\sin \Omega & 0 \\ \sin \Omega & \cos \Omega & 0 \\ 0 & 0 & 1 \end{pmatrix} \quad (2)$$

$$T_2 = \begin{pmatrix} 1 & 0 & 0 \\ 0 & \cos i & -\sin i \\ 0 & \sin i & \cos i \end{pmatrix} \quad (3)$$

$$T_3 = \begin{pmatrix} \cos u & -\sin u & 0 \\ \sin u & \cos u & 0 \\ 0 & 0 & 1 \end{pmatrix} \quad (4)$$

The argument of latitude u is calculated as the sum of the true anomaly ν and the argument of perigee ϖ :

$$u = \nu + \varpi \quad (5)$$

The orientation of the body frame with respect to the inertial frame is given by a quaternion, which is calculated by the filter that will be presented in Section 3.4.

3.2. Attitude representation and kinematics

The algorithm that will reconstruct the attitude of the spacecraft includes a mathematical model of the attitude kinematics of the satellite. In this section the filter embedded attitude representation and kinematics equations

will be introduced.

The attitude representation employed by the filter to represent the orientation from the ECEF frame to the body frame is dual. A quaternion representation is used to express the input, the output and the kinematic model inside the filter. A vector of generalized Rodrigues parameters is used in some numerical operations of the filter that might violate the unity norm property of the quaternion, otherwise.

The quaternion q is defined as

$$q = \begin{pmatrix} q_1 & q_2 & q_3 & q_4 \end{pmatrix}' = \begin{pmatrix} \bar{q} & q_4 \end{pmatrix}' \quad (6)$$

The kinematic equation associated to the quaternion is given by

$$\dot{q} = \frac{1}{2}\Xi(q(t))\omega(t) \quad (7)$$

where ω is the angular velocity vector of the satellite and Ξ is a matrix defined as

$$\Xi(q) = \begin{pmatrix} q_4 I_{3 \times 3} + \bar{q} \times \\ -\bar{q}^T \end{pmatrix} \quad (8)$$

where $\bar{q} \times$ is the cross-product matrix associated to the vector \bar{q} . Given the discrete-time nature of the application studied in this paper, a discrete-time version of Eq. 7 has to be introduced. The quaternion at the $k + 1^{th}$ step of the algorithm is

$$q_{k+1} = \Omega(\omega_k)q_k \quad (9)$$

with

$$\Omega(\omega_k) = \begin{pmatrix} Z_k & \psi_k \\ -\psi_k & \cos(0.5\|\omega_k\|\Delta t) \end{pmatrix} \quad (10)$$

$$Z_k = \cos(0.5\|\omega_k\|\Delta t)I_{3 \times 3} - \psi_k \times$$

$$\psi_k = \frac{\sin(0.5\|\omega_k\|\Delta t)\omega_k}{\|\omega_k\|}$$

where ω_k is the angular velocity vector, measured from the rate-gyros, and Δt the measurements sampling interval.

The quaternion is used to express the orientation of the body frame with respect to the orbital frame. This is done by defining a direction cosine matrix DCM equivalent to the quaternion and multiplying it by the T matrix defined in Eq. 1. The direction cosine matrix DCM obtained from a quaternion q is calculated as

$$DCM = \begin{pmatrix} 1 - 2(q_2^2 + q_3^2) & 2(q_1q_2 + q_3q_4) & 2(q_1q_3 - q_2q_4) \\ 2(q_1q_2 - q_3q_4) & 1 - 2(q_1^2 + q_3^2) & 2(q_2q_3 + q_1q_4) \\ 2(q_1q_3 + q_2q_4) & 2(q_2q_3 - q_1q_4) & 1 - 2(q_2^2 + q_4^2) \end{pmatrix} \quad (11)$$

A four-components quaternions is a non-singular representation of the special orthogonal group $SO(3)$ of three-dimensional rotation matrices which represents 3D attitude and it is therefore a redundant representation [20]. The multiplicative quaternion approach, commonly used in spacecraft attitude estimation problems, adopts this redundancy to represent the reference attitude free of singularity while the three components representation describes the deviation from this reference [21]. Therefore, the algorithm represents the attitude as the quaternion product

$$\begin{aligned} \bar{q} &= \delta q(\vec{v}) \times \bar{q}_{ref} \\ \delta q &= \begin{pmatrix} \delta \bar{q} & \delta q_4 \end{pmatrix} \end{aligned} \quad (12)$$

where \bar{q}_{ref} is the reference quaternion and the small deviation $\delta q(a)$ from \bar{q}_{ref} to the actual attitude q is parameterized by a three-component vector \vec{v} .

The error quaternion components are used to define the vector of generalized Rodrigues parameters δp

$$\delta p = f \frac{\delta \bar{q}}{a + \delta q_4} \quad (13)$$

where the parameter $a \in [0 \ 1]$ and f is a scale factor. For $a = 0$ and $f = 1$, Eq. 13 returns the Gibbs vector, while for $a = 1$ and $f = 1$ it gives the standard modified Rodrigues parameters. According to [11], the choice of $f = 2(a + 1)$ is a suitable pick and it will be adopted throughout this paper.

The inverse transformation from δp to δq is

$$\begin{aligned}\delta q_4 &= \frac{-a\|\delta p\|^2 + f\sqrt{f^2 + (1-a^2)\|\delta p\|^2}}{f^2 + \|\delta p\|^2} \\ \delta \bar{q} &= f^{-1}(a + \delta q_4)\delta p\end{aligned}\tag{14}$$

3.3. Measurements model

The available measurements on board Unisat-6 are the Earth magnetic field vector from the magnetometer and the spacecraft angular velocity vector from the rate-gyros.

The magnetometer measures the intensity of the Earth magnetic field along its three axes (see Fig. 1), that can be easily translated into the body axes (see Fig. 3). This vector can be compared with the information of the World Magnetic Model (WMM), which returns the intensity of the Earth magnetic field in the ECEF frame, thus giving information on the orientation of the body axes frame with respect to the ECEF frame. The noise on the measurement vector \vec{b} of the magnetometer is modeled as an additive Gaussian zero-mean white process with variance σ_m .

The rate-gyro measures the angular velocity ω of the satellite in the body frames. This measurement is usually modeled as [22]

$$\begin{aligned}\tilde{\omega}(t) &= \omega_{true}(t) + \beta(t) + \eta_v(t) \\ \dot{\beta}(t) &= \eta_u(t)\end{aligned}\tag{15}$$

where the true angular velocity ω_{true} is corrupted by a bias β , and η_v and η_u are two Gaussian zero-mean white processes with variances σ_v and σ_u , respectively.

3.4. Unscented attitude filter

The filter employed for UniSat-6 attitude reconstruction was first proposed in [11] and it was given the name of USQUE (UnScented QUaternion Estimator, which is also a Latin expression meaning ‘all the way’). The USQUE is an attitude-dedicated formulation of the Unscented filter. This section will present the algorithm of the filter employed in this work.

The USQUE, as well as the original formulation of the Unscented filter, is constituted by a prediction phase, in which the *a priori* estimate is constructed by averaging the values of a finite number of points from the state space (the σ -points), and by a correction phase, in which the *a priori* estimate is corrected with the information from the measurements. The USQUE algorithm employs the data from the rate-gyro in the prediction phase so as to calculate the kinematics of the satellite, while the magnetometer output is the only measurement employed in the correction phase.

The algorithm described in the following assumes a discrete-time nonlinear system, modeled as

$$\begin{aligned} x_{k+1} &= f(x_k, k) + G_k w_k \\ \tilde{y}_k &= h(x_{k,k}) + v_k \end{aligned} \tag{16}$$

where x_k is the state vector, \tilde{y}_k is the measurement vector, and w_k and v_k are zero-mean Gaussian noise vectors representing the process noise and the measurements noise with covariance matrices Q_k and R_k , respectively.

The state vector to be estimated is formed by the generalized Rodrigues

parameters and the biases of the rate-gyros.

$$\hat{x} = \begin{pmatrix} \delta p \\ \beta \end{pmatrix} \quad (17)$$

A quaternion can serve as an initial guess for the attitude, since it can be transformed into the vector of generalized Rodrigues parameters with Eq. 13. The filter is initialized with an initial guess for the state estimate \hat{x} and an initial value for the error covariance matrix P .

The algorithm starts with a step of the prediction phase. The σ -points at the k^{th} step are defined as:

$$\chi_k = \begin{bmatrix} \chi_k^{\delta p}(i) \\ \chi_k^\beta(i) \end{bmatrix}, \quad i = 0, 1, \dots, 2n \quad (18)$$

with n being the size of the state vector. In the σ -points partitioning, $\chi_k^{\delta p}$ represents the attitude-error part and χ_k^β the gyro bias part. The $2n + 1$ σ -points depend on the actual value of the estimated state \hat{x}_k^+ and of the error covariance matrix P_k^+ and are chosen from the columns of the matrix M :

$$M = \hat{x}_k^+ + \begin{bmatrix} 0_n & S & -S \end{bmatrix} \quad (19)$$

$$S = \sqrt{(n + \lambda)(P_k^+ + Q_k)}$$

in which λ is a tuning parameter of the filter which tells how much the σ -points are spread around the mean. In order to propagate the attitude, the $\chi_k^{\delta p}$ are transformed into correspondent quaternion deviations δq_k^+ , by means of Eq. 14. These deviations are used as in Eq. 12 to form a set of attitude quaternions spread around the mean \hat{q}_k^+ . The resulting set is

$$\hat{q}_k^+(0) = \hat{q}_k^+ \quad (20)$$

$$\hat{q}_k^+(i) = \delta q_k^+(i) \times \hat{q}_k^+, \quad i = 1, \dots, 2n$$

The first of these equations implies that $\chi_k^{\delta p}(0)$ be zero. Therefore, this reset is to be performed at each step of the algorithm.

Once that the quaternion representation of the σ -points has been calculated, the attitude can be propagated using the discrete kinematics of Eq. 9, where the angular velocity to be used is the estimated quantity $\hat{\omega}_k^+$:

$$\hat{\omega}_k^+(i) = \tilde{\omega}_k - \chi_k^\beta(i), \quad i = 0, 1, \dots, 2n \quad (21)$$

After the propagation of the quaternions, the propagated Rodrigues parameters can be obtained back by using Eq. 13, where the error quaternions are obtained once again by applying Eq. 12. At the end of the prediction phase, the propagated σ -points are

$$\begin{aligned} \chi_{k+1}^{\delta p}(0) &= 0 \\ \chi_{k+1}^{\delta p}(i) &= f \frac{\delta \bar{q}_{k+1}(i)}{a + \delta q_{k+1}(i)}, \quad i = 1, 2, \dots, 2n \\ \chi_{k+1}^\beta(i) &= \chi_k^\beta(i), \quad i = 0, 1, \dots, 2n \end{aligned} \quad (22)$$

The predicted state vector \hat{x}_{k+1}^- is computed as

$$\hat{x}_{k+1}^- = \frac{1}{n + \lambda} \left\{ \lambda \chi_{k+1}(0) + \frac{1}{2} \sum_{i=1}^{2n} \chi_{k+1}(i) \right\} \quad (23)$$

The predicted error covariance matrix is calculated as

$$\begin{aligned} P_{k+1}^- &= \frac{1}{n + \lambda} \left\{ \lambda [\chi_{k+1}(0) - \hat{x}_{k+1}^-] [\chi_{k+1}(0) - \hat{x}_{k+1}^-]^T \right. \\ &\quad \left. + \frac{1}{2} \sum_{i=1}^{2n} [\chi_{k+1}(i) - \hat{x}_{k+1}^-] [\chi_{k+1}(i) - \hat{x}_{k+1}^-]^T \right\} + Q_k \end{aligned} \quad (24)$$

The mean observation is given by

$$\hat{y}_{k+1}^- = \frac{1}{n + \lambda} \left\{ \lambda \gamma_{k+1}(0) + \frac{1}{2} \sum_{i=1}^{2n} \gamma_{k+1}(i) \right\} \quad (25)$$

where $\gamma_{k+1}(i)$ are the measurements obtained by applying the h function from Eq. 16 to the set $\chi_{k+1}(i)$.

The innovation covariance matrix is given by

$$P_{k+1}^{\nu\nu} = \frac{1}{n + \lambda} \left\{ \lambda [\gamma_{k+1}(0) - \hat{y}_{k+1}^-] [\gamma_{k+1}(0) - \hat{y}_{k+1}^-]^T + \frac{1}{2} \sum_{i=1}^{2n} [\gamma_{k+1}(i) - \hat{y}_{k+1}^-] [\gamma_{k+1}(i) - \hat{y}_{k+1}^-]^T \right\} + R_{k+1} \quad (26)$$

The cross-correlation matrix is given by

$$P_{k+1}^{xy} = \frac{1}{n + \lambda} \left\{ \lambda [\chi_{k+1}(0) - \hat{x}_{k+1}^-] [\gamma_{k+1}(0) - \hat{y}_{k+1}^-]^T + \frac{1}{2} \sum_{i=1}^{2n} [\chi_{k+1}(i) - \hat{x}_{k+1}^-] [\gamma_{k+1}(i) - \hat{y}_{k+1}^-]^T \right\} \quad (27)$$

The correction phase consists in the update of the predicted state vector x_{k+1}^- and of the error covariance matrix P_{k+1}^-

$$\hat{x}_{k+1}^+ = \hat{x}_{k+1}^- + K_k v_k \quad (28)$$

$$P_{k+1}^+ = P_{k+1}^- - K_k P_k^{vv} K_k^T \quad (29)$$

where v_k is the innovation and K_k the Kalman gain, given by, respectively

$$v_k = \tilde{y}_k - h(\hat{x}_k^-, k) \quad (30)$$

$$K_k = P_k^{xy} (P_k^{\nu\nu})^{-1} \quad (31)$$

The process noise covariance matrix Q_k is actualized at each time step, since the measurements sampling time is not constant. According to [11], the matrix is defined as

$$Q_k = \frac{\Delta t}{2} \begin{pmatrix} (\sigma_v^2 - \frac{1}{6}\sigma_u^2\Delta t^2)I_{3\times 3} & 0_{3\times 3} \\ 0_{3\times 3} & \sigma_u^2 I_{3\times 3} \end{pmatrix} \quad (32)$$

At the k^{th} step the filter provides the estimation vector \hat{x}_k and the matrix P_k .

4. Results

This section describes the results of attitude reconstruction performed starting from the UniSat-6 flight data as received by the GAUSS ground station in Roma. These data include telemetry of the satellite and data from the sensors that were stored along a time interval of more than 26 hours, which corresponds to approximately 18 orbits of UniSat-6 around the Earth. These operations were performed on April 24th-25th, 2015 with the initial time instant t_0 at 20:51 UTC of April 24th. Data sampling rate is variable, since the on-board computer does not give a clock for the measurements. Most of the measurements occur with a time interval of 4-6 seconds.

The initial guess for the attitude corresponds to the first measurement from the magnetometers, while a value of $0.1 \cdot \pi/180$ is assumed for the three gyro biases. The error covariance matrix P is initialized with the variances of the magnetometers and of the gyro biases. The value of λ was chosen to be equal to 0.05.

Fig. 4 shows the measurements history from the \hat{x}_b axis rate-gyro. It can be seen that, during the considered time interval, there are two periods in which measurements are much more frequent (areas in which circles are denser). At t_0 , UniSat-6 was in a normal operation mode with data sampling every 30 seconds. A high-frequency measurements mode was set up for UniSat-6 almost an hour after t_0 , at 21:44 UTC. Six hours later, at 4:18 UTC, the satellite autonomously returned to the normal operation mode with measurements every 30 seconds, due to a radiation event which caused a re-start of the system. Four hours later, the high-frequency mode was manually re-established from ground by GAUSS operators. This high-frequency mode was kept until

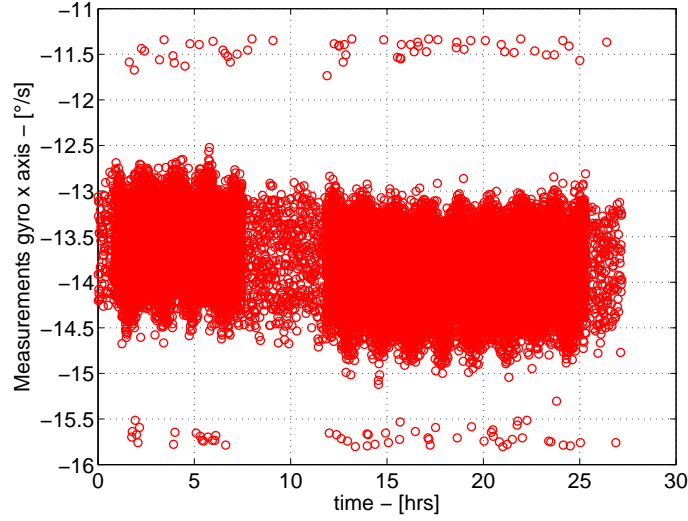


Figure 4: \hat{x}_b axis gyro measurements

22:10 UTC. A normal operation mode interval closes the sequence of data until 0:00 UTC.

Figs. 5 and 6 show the results of the estimated Euler angles of roll ($\hat{\phi}$) and pitch ($\hat{\theta}$). These angles, as well as the yaw angle ($\hat{\psi}$) that will be analyzed later, are obtained by transforming the quaternion calculated as output of the filter with the procedure described in Section 3.2. The superimposed $\hat{\cdot}$ symbol indicates that these variables are estimated.

It can be seen that $\hat{\phi}$ and $\hat{\psi}$ angles oscillate within a certain range of values. The roll angle varies mainly between 0° and 100° . The pitch angle varies mainly between 0° and 60° . These rotations are very fast, in the order of 4-5 *rpm*. The result of these oscillations is a three-dimensional elliptical cone described from the spacecraft. The size of the two axes of the ellipse at the base is equivalent to the angular oscillations of roll and pitch. Therefore, the

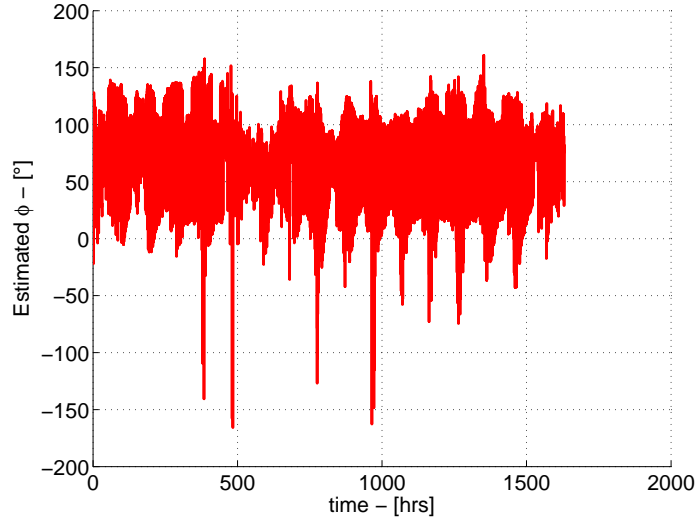


Figure 5: **Estimated ϕ angle**

aperture of the cone is variable.

Comparing the results of Fig. 6 with those of Fig. 4, it can be seen that the amplitude of the periodical variations is diminished when the satellite goes in the normal operation mode. The results of attitude reconstruction are degraded with this mode. This is reasonable, since these measurements have a higher sampling time although the satellite is still rotating fast. Nevertheless, the algorithm is still able to satisfactorily estimate the attitude of the satellite. Furthermore, the degradation of the results is visible only in the reconstruction of the pitch angle. This is a first indication of the robustness of the filter.

The most interesting information on the attitude motion of UniSat-6 can be derived from the observation of the yaw motion. The estimated yaw angle $\hat{\psi}$ is shown in Fig. 7 and it can be seen that it oscillates periodically

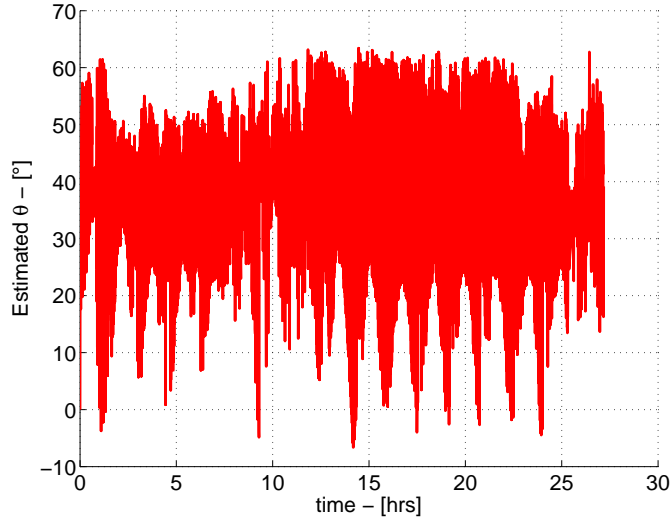


Figure 6: **Estimated θ angle**

between -180° and 180° . Fig. 8 shows a sample of the $\hat{\psi}$ history concerning two consecutive orbits. In particular, the selected orbits pass over the North and South magnetic poles with the closest approximation among all the considered orbits. The circles and the diamonds approximately indicate the passages over the North and the South Magnetic Pole, respectively. Remembering that, by definition, the yaw angle defined in Fig. 2 is the angle between \hat{r} and the projection of \hat{x}_b on the orbital plane, an interesting result about the attitude motion can be derived.

At the passage over the North magnetic pole (located at approximately 80° of latitude North), it can be seen that the value of $\hat{\psi}$ is close to zero. This means that the projection of the \hat{x}_b axis is almost aligned to the orbit radius. It is well known that, over the magnetic poles, the Earth magnetic field lines are perpendicular to the surface of the Earth. Therefore, the \hat{x}_b axis, on the

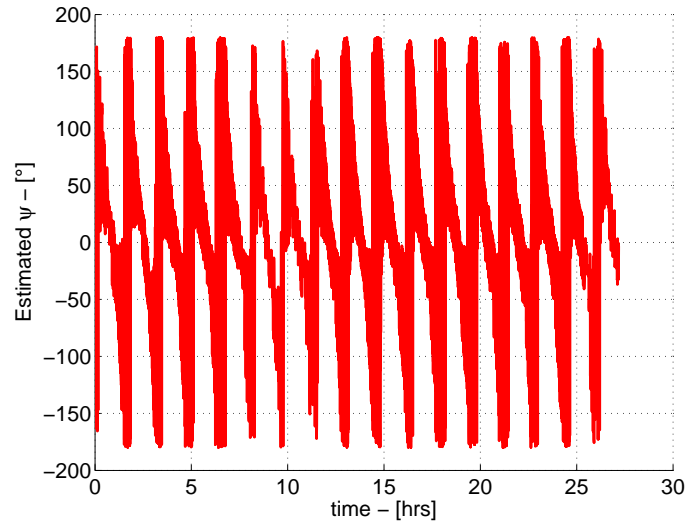


Figure 7: Estimated ψ angle

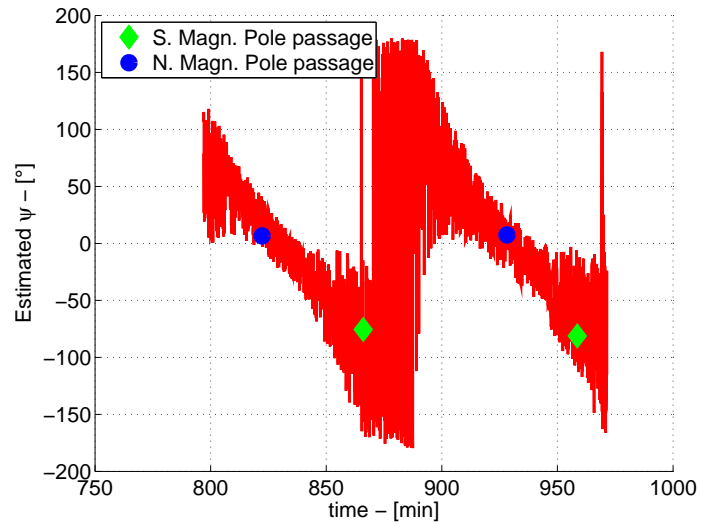


Figure 8: Detail of the estimated ψ angle

orbital plane, is aligned with the lines of the Earth magnetic field.

Continuing towards the South magnetic pole, the value of $\hat{\psi}$ decreases slowly, until it reaches almost -90° right before reaching the South magnetic pole (located at approximately -60° of latitude South). Right after the passage over the South magnetic pole, the value of $\hat{\psi}$ passes abruptly from -90° to -180° and rises eventually to 180° . After reaching the 180° halfway the path from the South to the North magnetic pole, $\hat{\psi}$ starts decreasing again, until it reaches a value of almost 0° over the North magnetic pole.

This behavior suggests that the \hat{x}_b axis has been aligned to the lines of the Earth magnetic field due to the magnetization of the hysteresis rod along \hat{x}_b . A perfect alignment with the lines of the Earth magnetic field would have implied $\psi = -180^\circ$ above the South magnetic pole (lines of the magnetic field going out from the Earth – see also Fig. 9). Nevertheless, the use of a passive magnetic attitude control system does not guarantee this perfect alignment, but only a coarse one. Furthermore, because of the not symmetric distribution of the magnetic poles on the surface of the Earth, the path from the North to the South magnetic pole is shorter than the one from South to North for the considered orbits. Therefore, when traveling from North to South, the \hat{x}_b axis has less time to complete the -180° rotation of the lines of the Earth magnetic field. This is why the spacecraft experiences a big yaw rotation right after the passage above the South magnetic pole.

The contribution of the other magnetic devices (permanent magnets along \hat{y}_b , hysteresis rods along \hat{y}_b and \hat{z}_b) can be neglected. The contribution of the hysteresis rod along the \hat{y}_b axis is equivalent only to $1/8$ of the effect of the \hat{x}_b axis hysteresis rod. The magnets placed along the \hat{y}_b axis and the

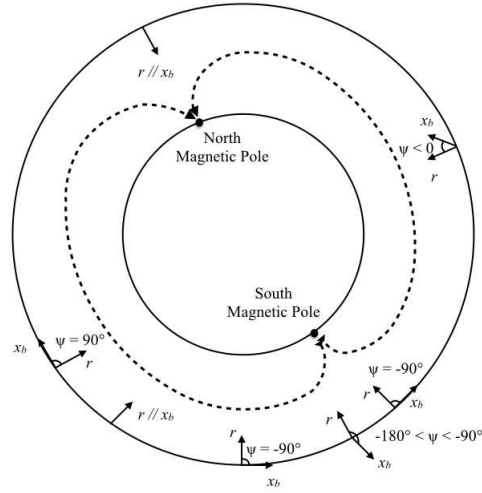


Figure 9: Yaw orientation along the orbit

hysteresis rods along the \hat{z}_b axis are not effective. The average effect of the magnetic torque produced by them, calculated on a full rotation, is, in fact, zero. Since the rotations of roll and pitch are much faster than those of yaw (3-5 *rpm* against 0.01 *rpm*), the average torque of the formers goes rapidly to zero. In order for the devices along \hat{y}_b and \hat{z}_b to work, UniSat-6 should have been equipped with a detumbling control to stop the initial rotations. A small variation in the amplitude of the yaw variation can be seen in the fifth orbit of Fig. 7, when the yaw arrives only at 160° and not at 180° . This is in correspondence with the normal operation mode when there available measurements have a higher sampling time.

In conclusion, the attitude motion of UniSat-6 is composed of two dynamics, a long period one and a short period one. The long period motion consists of two 360° yaw rotations completed in one orbit, which makes the \hat{x}_b axis following the Earth magnetic field lines. The short period motion is given by



Figure 10: **25 s sequence of pictures from the on-board camera**

the fast oscillations (up to 5 *rpm*) of roll and pitch, which describe a variable aperture elliptical cone in space.

These data are consistent with the images taken from the camera of UniSat-6, placed on top the \hat{y}_b panel. Several images were taken both in the direction of the Earth and in the direction of the outer space, as it is shown in Fig. 10. This figure is composed of 18 pictures taken from the camera between April 25, 2015 10:17:29 UTC and April 25, 2015 10:17:54 UTC. In the first picture, the camera is pointing towards the Sun; then, it is pointing towards the Earth (pictures 7 to 13); eventually, it points towards the Sun again. The panel with the camera (\hat{y}_b axis), therefore, describes a cone in space.

5. Conclusions

This paper has presented the results of the attitude determination of the UniSat-6 satellite. The estimation was realized analyzing real data collected on-board the spacecraft and processed at ground.

Data from the rate-gyro and magnetometers were processed using the USQUE algorithm. The results show that the spacecraft has a coarse alignment of

its \hat{x}_b axis to the lines of the Earth magnetic field, while the two other axes rotate in space with a period of 5 *rpm*.

Due to a problem on the on-board electronics caused by a radiation event, the spacecraft was not able to collect data with the expected sampling rate (30 *s* instead of 4 *s*) for six hours. Nevertheless, in this interval the filter was able to reconstruct the attitude of the spacecraft with almost the same accuracy as before. The reconstructed attitude of the spacecraft is consistent with the images taken from the on-board camera.

References

- [1] J. A. Vilán, F. Aguado Agelet, M. López Estévez, A. González Muiño, Flight results: Reliability and lifetime of the polymeric 3d-printed antenna deployment mechanism installed on xatcobeo & humsat-d, *Acta Astronautica* 107 (2015) 290–300.
- [2] B. Malphrus, M. Combs, J. Kruth, K. Brown, B. Twiggs, E. Thomas, T. Rose, University-based nanosatellite missions and ground operations at morehead state.
- [3] A. Nascetti, E. Pittella, P. Teofilatto, S. Pisa, High-gain s-band patch antenna system for earth-observation cubesat satellites, *Antennas and Wireless Propagation Letters, IEEE* 14 (2015) 434–437.
- [4] M. Pontani, C. Cappelletti, Cubesat collision risk analysis at orbital injection, in: *Advances in Astronautical Sciences, Proceedings of the 23rd AAS/AIAA Space Flight Mechanics Meeting, Vol. 148*, American Astronautical Society, 2013, pp. 3111–3130.

- [5] B. Klofas, Upcoming amateur radio cubesats: The flood has arrived, Paper presented at the 2013 AMSAT Annual Meeting and Space Symposium, Houston, Texas, USA (2013).
- [6] B. Klofas, Cubesat communications update, Paper presented at the CubeSat 2014 Summer Workshop, Logan, Utah, USA (2014).
- [7] C. Paris, M. Parisse, A. Nascetti, R. Cica, N. A. Salman, The tigrisat camera a nanosatellite optical payload for detecting dust and sand storms, in: Environment and Electrical Engineering (EEEIC), 2015 IEEE 15th International Conference on, IEEE, 2015, pp. 1605–1610.
- [8] J. L. Crassidis, F. L. Markley, Y. Cheng, Survey of nonlinear attitude estimation methods, *Journal of Guidance, Control, and Dynamics* 30 (1) (2007) 12–28.
- [9] J. L. Farrell, Attitude determination by kalman filtering, *Automatica* 6 (3) (1970) 419–430.
- [10] E. J. Lefferts, F. L. Markley, M. D. Shuster, Kalman filtering for spacecraft attitude estimation, *Journal of Guidance, Control, and Dynamics* 5 (5) (1982) 417–429.
- [11] J. L. Crassidis, F. L. Markley, Unscented filtering for spacecraft attitude estimation, *Journal of guidance, control, and dynamics* 26 (4) (2003) 536–542.
- [12] J. Uhlmann, S. Julier, H. Durrant-Whyte, A new method for the non linear transformation of means and covariances in filters and estimations, *IEEE Transactions on automatic control* 45.

- [13] P. Sekhavat, Q. Gong, I. Ross, Unscented kalman filtering: Npsat1 ground test results, in: AIAA Guidance, Navigation, and Control Conference, Keystone, Colorado, 2006.
- [14] J.-W. Kim, J. L. Crassidis, S. R. Vadali, A. Dershowitz, International space station leak localization using attitude response data, *Journal of guidance, control, and dynamics* 29 (5) (2006) 1041–1050.
- [15] G. Figueiró de Oliveira, P. H. Dória Nehme, C. Cappelletti, Analysis and simulation of attitude determination and control for the serpens nanosatellite, in: *Proceedings of the 2nd IAA Conference on Dynamics and Control of Space Systems*, International Academy of Astronautics, 2014.
- [16] A. Nascetti, D. Pancorbo-D’Ammando, M. Truglio, Abacus advanced board for active control of university satellites, in: *Proceedings of the 2nd IAA Conference on University Satellite Missions and Cubesat Workshop*, International Academy of Astronautics, 2013.
- [17] S. Paiano, M. Truglio, A. Conde Rodriguez, C. Cappelletti, F. Graziani, Unisat-6 mission, in: *Proceedings of the 1st Latin American IAA Cubesat Workshop*, International Academy of Astronautics, 2014.
- [18] M. Truglio, A. Conde Rodriguez, C. Cappelletti, F. Graziani, Unisat-6: Mission results and lesson learned about an innovative multipurpose micro satellite, in: *Proceedings of the 66th International Astronautical Congress*, International Astronautical Federation, 2015.

- [19] A. Conde Rodriguez, M. Truglio, F. Graziani, C. Cappelletti, Microsatellites ground operations and best practices from the experience of unisat-6, in: Proceedings of the 66th International Astronautical Congress, International Astronautical Federation, 2015.
- [20] F. L. Markley, Multiplicative vs. additive filtering for spacecraft attitude determination, in: Proceedings of the 6th Conference on Dynamics and Control of Systems and Structures in Space (DCSSS), Vol. 22, 2004.
- [21] F. L. Markley, Attitude error representations for kalman filtering, Journal of guidance, control, and dynamics 26 (2) (2003) 311–317.
- [22] R. Farrenkopf, Analytic steady-state accuracy solutions for two common spacecraft attitude estimators, Journal of Guidance, Control, and Dynamics 1 (4) (1978) 282–284.